Characterizing The Failure of Parachute Seams:
The Impact of Stitch Concentration and Strain Rate on Ultimate Tensile Strength

by

Pavlina Karafillis

Submitted to the
Department of Mechanical Engineering
in Partial Fulfillment of the Requirements for the Degree of

Bachelor of Science in Mechanical Engineering

at the

Massachusetts Institute of Technology

June 2017

MASSACHUSETTS INSTITUTE OF TECHNOLOGY
JUL 25 2017
LIBRARIES
ARCHIVES

© 2017 Massachusetts Institute of Technology. All rights reserved.

Signature of Author: Signature redacted
Department of Mechanical Engineering
May 19, 2014

Certified by: Signature redacted
Jeehwan Kim
Assistant Professor, Department of Mechanical Engineering
Thesis Supervisor

Accepted by: Signature redacted
Rohit Karnik
Professor of Mechanical Engineering
Undergraduate Officer

Characterizing The Failure of Parachute Seams:
The Impact of Stitch Concentration and Strain Rate on Ultimate Tensile Strength

by

Pavlina Karafillis

Submitted to the Department of Mechanical Engineering
on May 19, 2017 in Partial Fulfillment of the
Requirements for the Degree of

Bachelor of Science in Mechanical Engineering

ABSTRACT

Parachutes are commonly used in space mission landings. With increasing payloads, parachutes are getting larger, bearing larger loads and operating at faster speeds. Designing these devices requires a knowledge of aerodynamics, fluid flow, and the mechanical properties of cloth. A brief overview of the basics of parachute design are described. There are many possible failure modes, but catastrophic failures are caused by failures at the weakest point of the parachute, the seam.

Seams are characterized by a seam efficiency, a percentage of the strength of the cloth used to stitch the seam together. In this study, seams and cloth were tested to failure on an Instron 5582 to experimentally determine their respective Ultimate Tensile Strengths (UTS). The ratio of the seam UTS to the cloth UTS was used to determine seam efficiency. Results indicated no clear relationship between strain rate and seam efficiency in the range tested. However, a strong relationship between stitch concentration and seam efficiency was established. A best fit curve was developed and with an an R^2=0.80.

In order to better understand the failure mode, the open source Matlab function Ncorr was also used to provide a visualization of the strain on the coupons during testing. The results of the digital correlation analysis performed by Ncorr are also reported, and indicate the importance of transverse and shear strain in causing catastrophic failure.

Thesis Supervisor: Jeehwan Kim
Title: Characterizing The Failure of Parachute Seams: The Impact of Stitch Concentration and Strain Rate on Ultimate Tensile Strength

Acknowledgements

I would like to thank Barbara Hughey for organizing this project, as a part of the MIT undergraduate class 2.671 – Measurement and Instrumentation, and for being a wonderful resource throughout the work of this thesis. I would also like to thank Pierce Hayward for allowing me to use the Instron for the tensile experiments, and for assisting me in the use of both the Instron and Vic2D. Last, but certainly not least I would like to thank Professor Jeehwan Kim, my thesis advisor, for providing valuable insight and feedback throughout the project.

Table of Contents

Abstract 3

Acknowledgements 5

Table of Contents 6

List of Figures 7

List of Tables 8

1. Introduction 9

1.1 Parachute History and Uses 9

1.2 Parachute Types and Design 9

1.2.1 Disk Band Gap 9

1.2.2 Ringsail 10

1.2.3 Rogallo Wing 11

1.2.4 Basic Design Guidelines 11

2. Background 13

2.1 Failure Stress and Von Mises Stress 13

2.2 Accurately Assessing Ultimate Tensile Strength 13

2.3 Stress Concentration 14

2.4 Thread Failure 14

3. Experimental Design 14

3.1 Sample Fabrication 14

3.2 Instron Testing 14

3.3 Vic-Snap 2010 and Ncorr Setup 15

4. Results 15

4.1 Instron Data 14

4.2 Vic-Snap 2010 and Ncorr Visualizations 14

5. Discussion 27

5.1 Instron Data 27

5.2 Ncorr and Images 27

6. Conclusions 28

7. References 29

List of Figures

Figure 1-1: Disk Band Gap Parachute 9

Figure 1-2: Ringsail Parachute 10

Figure 1-3: Rogallo Wing 11

Figure 1-4: Seam Failure 12

Figure 3-1: Sample Fabrication 14

Figure 3-2: Sample Stitch Concentration 15

Figure 3-2: Instron Testing 15

Figure 4-1: Seam Efficiency vs. Strain Rate 16

Figure 4-2: Seam Efficiency vs. Number of Stitches per Inch 16

Figure 4-3: Transverse Green-Lagrangian Strain – (29.2 stitches per inch) 18

Figure 4-4: Shear Green-Lagrangian Strain – (29.2 stitches per inch) 18

Figure 4-5: Longitudinal Green-Lagrangian Strain – (29.2 stitches per inch) 19

Figure 4-6: Transverse Green-Lagrangian Strain – (15.4 stitches per inch) 19

Figure 4-7: Shear Green-Lagrangian Strain – (15.4 stitches per inch) 20

Figure 4-8: Longitudinal Green-Lagrangian Strain – (15.4 stitches per inch) 20

Figure 4-9: Transverse Green-Lagrangian Strain – (8.67 stitches per inch) 21

Figure 4-10: Shear Green-Lagrangian Strain – (8.67 stitches per inch) 21

Figure 4-11: Longitudinal Green-Lagrangian Strain – (8.67 stitches per inch) 22

Figure 4-12: Strain Visualization at Failure-(29.2 stitches per inch) 24

Figure 4-13: Strain Visualization at Failure-(15.4 stitches per inch) 25

Figure 4-14: Strain Visualization at Failure-(8.67 stitches per inch) 26

Figure 5-1: Comparison of Stitch Sizes Before Failure 27

List of Tables

TABLE 4-1: Failure Mode of the Seam 23

TABLE 4-2: Failure Mode of the Seam 26

1 Introduction

1.1 Parachute History and Uses

The first documentation of the concept of a structured fabric that would induce drag was in an anonymous manuscript from the 1470s. In 1485, Leonardo da Vinci designed a parachute that would be built and tested centuries after his death, in 2000, by extreme sport enthusiast Adrian Nichols. The inventor of the modern parachute is considered to be Louis-Sébastien Lenormand, who in 1783 completed the first documented jump with a parachute.[1]

In the 1900s, parachutes began to be used for a variety of military applications, including decelerating planes on short landing strips, and as a method of safe landing for a pilot that had been shot down. The low weight, low volume, and low cost of parachute makes them an extremely appealing device for flight related applications.

As a result, they were quickly adopted by space programs around the world. Parachutes have been used in dozens of missions, often in combination with thrusters, airbags, or other mechanisms, in order to provide a smooth landing for valuable scientific or even human cargo, or as an emergency landing systems for manned flights. With increasing payloads the parachutes are getting larger, bearing larger loads and operating at faster speeds. They have been used on Venus, Earth, Mars, Jupiter and Saturn's moon Titan.[2]

1.2 Parachute Types

Since their invention in 1783, parachutes have been adapted for industrial, military, and recreational applications. The space industry however has focused on two main designs: the Disc- Gap Band (DGB) and the Ringsail parachute.

1.2.1 Disk Gap Band

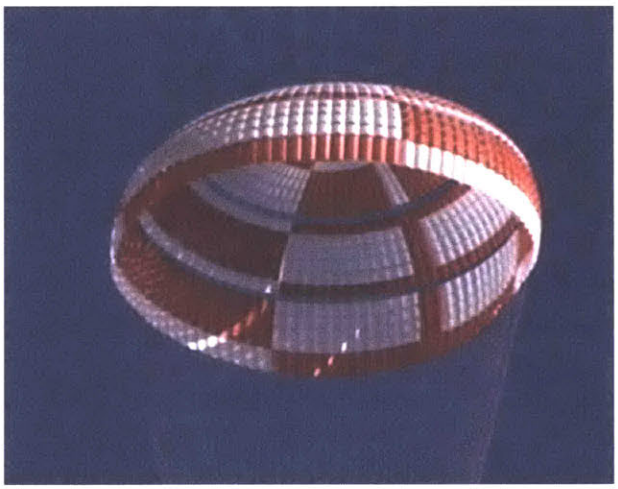


https://www.nasa.gov/mission_pages/mars/images/msl0153-20090422.html

Figure 1-1: A Disk Gap Band (DGB) parachute, aptly named after its structure containing a disk, a gap, and then a band. DGB parachutes are flight tested designs that have been used repeatedly in missions to Mars, and other planets.

DGB parachute design is named after its three characteristic components, a disk followed by a gap, and then then a band of cloth. The DGB is a well characterized and tested design. It has been recorded to inflate at speeds as high as Mach 3, and the areas of missing material make it lighter than other designs, both of which are favorable features for spaceflight. As a result, it has been used in all extraterrestrial planetary entry to date.[3] For a recent mission to Mars, the Mars Science Laboratory (MSL), a 51 foot wide and 165 foot long parachute was tested in a wind tunnel, in order to achieve deployment at up to Mach 2.2 on the Martian surface. However, this mission is a perfect example of the inability of parachutes to keep up with increasing loads of space missions. The parachute decelerated the capsule until a powered deceleration system known as the "sky crane" kicked in, slowing the capsule so it can be dropped onto the surface with a tether.[4]

1.2.2 Ringsail

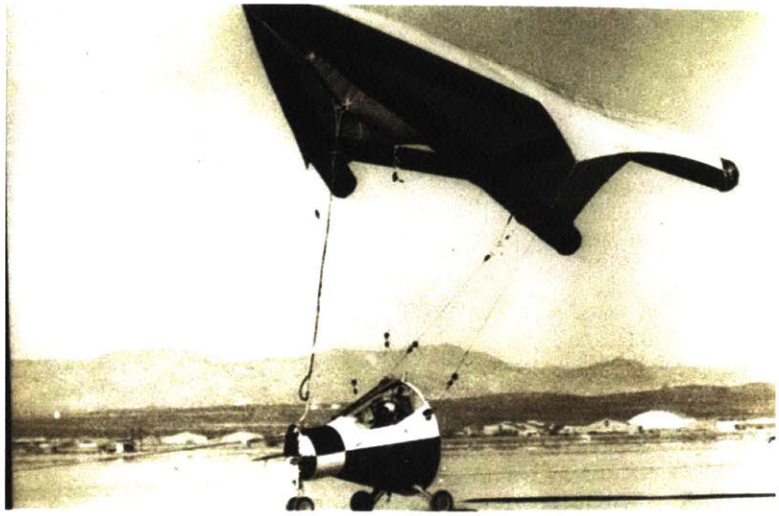


https://www.jpl.nasa.gov/news/news.php?feature=4604

Figure 1-2: A Ringsail parachute used in testing for the experimental Low Density Supersonic Decelerator (LDSD).[4] The rings that give the Ringsail parachute its name are clearly visible and sometimes even emphasized by changes in color from orange to white. The small gaps assist in letting air exit the parachute.

The Ringsail parachute consists of rings of cloth that are sewn in succession to create the characteristic parachute shape. These pieces, however are not sewn together necessarily at the edges but with small gaps between each ring in order to allow air to exit the parachute. Ringsail parachutes have yet to be successful in supersonic applications, but they have been used in several mission for terrestrial low speed landings. Ringsail parachutes are part of a more generic category of "slotted" parachutes, which have rings of cloth in succession with various types of spacing allowing air to exit the parachute.[5]

1.2.3 Rogallo Wing



https://www.flickr.com/photos/sdasmarchives/7142974799

Figure 1-3: The Rogallo wing during testing when it was under consideration for the Gemini mission.

The Rogallo Wing is an experimental design, championed by Gertrude Rogallo and her husband, NASA engineer Francis Rogallo. It has been considered for several missions as a replacement for more traditional designs, but was ultimately set aside after testing. It was patented by the Rogallos and was sold as a kite. Its simple design and construction make it applicable for a variety of recreational applications.[6]

1.2.4 Basic Design Guidelines

While each parachute type has its own design challenges and specialties, understanding the basics of sizing a parachute requires only basic knowledge of fluid mechanics and mechanics of materials. In order to determine the correct sizing, the mass of the desired load m and the desired velocity of descent v must be known. The force exerted by gravity must then be set equal to the force exerted by the parachute.

$$\rho \frac{\pi d^2}{4} C_D \frac{v^2}{2} = mg \qquad (1)$$

where ρ is the density of the air, d is the diameter of the parachute, g is the acceleration of gravity, m is the mass of the load, and the velocity of descent is v. C_D is the coefficient of drag, defined as

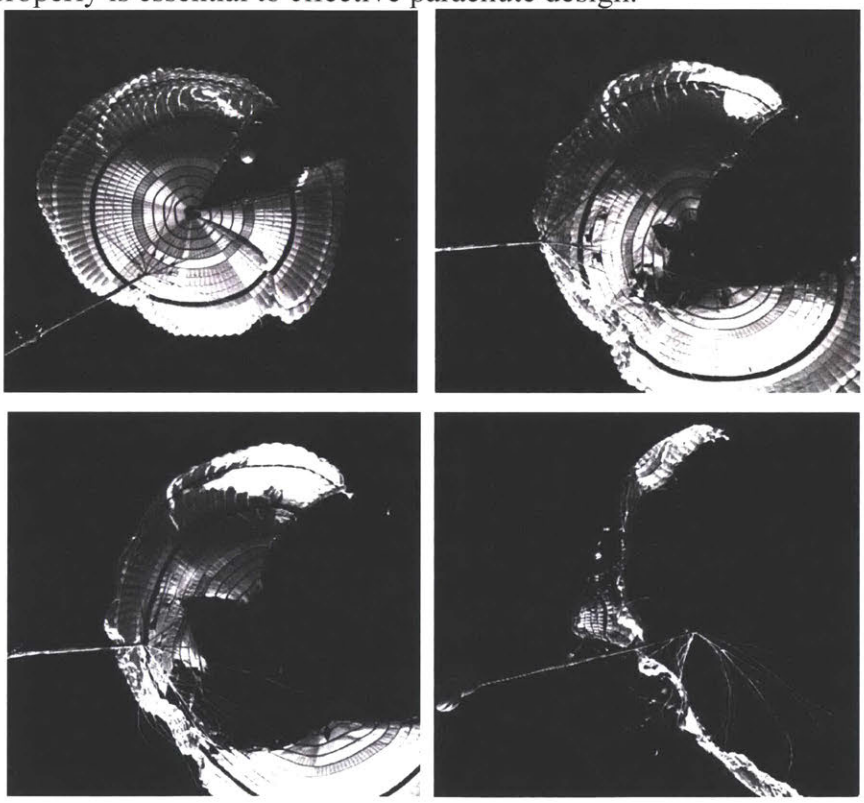
$$C_D = \frac{D}{A\rho\frac{v^2}{2}} \qquad (2)$$

where D is the drag force and A is the area of the application. C_D can be only empirically determined, however there are approximate values recorded for various parachute types that can be used in initial designs.

Once the parachute has been correctly sized, then the stresses on the parachute can be determined. The hoop stress of a hemispherical parachute is

$$\sigma = \frac{Pr}{2t} \tag{3}$$

where σ is the hoop stress, P is the applied pressure, r is the radius of the parachute, and t is the thickness of the parachute. The proper materials and manufacturing techniques must be selected to withstand these stresses.[7] Due to the curved nature of most parachutes, seams are required to create the geometry out of flat cloth. Seams are unique locations in a parachute that experience stresses from both the air pressure in the canopy, and the load being delivered. During testing, seams are often locations of catastrophic failure, as shown in **Figure 1-4.** Understanding and modeling them properly is essential to effective parachute design.



https://arc.aiaa.org/doi/pdf/10.2514/6.2016-3242

Figure 1-4: Failure of a supersonic Ringsail parachute in testing for the experimental deceleration system LDSD (Low Density Supersonic Decelerator). The failure shown here is directly after initial deployment. The failure of the seam in the top left image eventually leads to the complete dissolution of the parachute.

There are several different types of design choices that affect the seam, ranging from the materials used, to the type of stitch, to the number of stiches per inch, or even orientation of the cloth.[5]

2. Background

2.1 Failure Stress and Von Mises Stress

The failure strength of seams is essential to properly designing a parachute. Seam strength is often characterized in terms of seam efficiency,

$$S = \frac{s_s}{s_c} \tag{4}$$

where S is the seam efficiency, s_s is the maximum tensile load of the seam, and s_c is the maximum tensile load of the cloth.[8,9,10] While load is easy to measure, the exact same ratio can also be found with stress, since

$$\sigma_s = \frac{s_s}{A_s}, or\ \sigma_c = \frac{s_c}{A_c} \tag{5}$$

where and A_s is the area the load s_s is applied over on the seam, and A_c is the area the load s_c is applied over on the cloth. The seam is a system composed of both cloth and thread, but the cloth is the failure point, therefore A_s=A_c. Using distortion energy theory, the Von Mises stress can be used to predict the failure of a material in various stress states. The Von Mises stress must be less than the UTS in order for the design not to fail catastrophically. The equation for Von Mises Stress with only planar loads is

$$\sigma_v = \sqrt{{\sigma_1}^2 - \sigma_1\sigma_2 + {\sigma_2}^2 + 3{\sigma_{12}}^2} \tag{6}$$

where σ_v is the Von Mises stress, σ_1 is the stress in one axis, σ_2 is the stress in the perpendicular planar axis, and σ_{12} is the shear stress.

After determining the UTS in Newtons, the area of the cloth sample must be determined to calculate stress in Pascals. In this study, the width of each sample was measured with calipers in five separate locations along the coupon prior to testing. The thickness of the cloth was determined by taking thirty-six measurements of the thickness of the cloth purchased with a micrometer and using the average as the thickness, which was (3.15± .06)E-03 inches.

2.2 Accurately Assessing Ultimate Tensile Strength

One concern of this study, is properly assessing the UTS of the sample, due to the inherent directionality of fabric. Typically in fabric there is a warp direction, the direction in which the primary threads of the fabric are oriented, and the weft, the direction that the threads with are woven around the primary threads. As a result, fabric is often anisotropic, with different material properties in each direction.[11] In this study, only one direction, the warp direction, is assessed, leaving a framework for the weft testing and a possibility for future work. However, since the samples are manually assembled and placed into the Instron, there was a possibility that if these samples are sewn together at an angle, or placed in the Instron at an angle, the UTS recorded would be faulty, and would be a function of the percentage of the load in the weft direction rather than a function of either the strain rate or the stitch concentration. As a result, the UTS of the warp and the weft of the nylon cloth were characterized, using the same procedure as shown in **Section 3.1**. The UTS of the weft direction was (1.132 ±.062)E07 Pa, and the UTS in the warp direction was (1.418±.049)E07 Pa. A T-Test with a value of p=2.2E-06 confirms that this material is anisotropic in these two directions. However, the weft has a UTS that is 79.8% of the warp direction. Given that all manual alignment will be accurate to within ±10 degrees, this

means that this anisotropy will cause an error of less than 1%, which for the purposes of this study, is acceptable.

2.3 Stress Concentration

The predicted form of failure is at the intersection of the nylon thread, and the cloth. There, the thread will pull on the cloth and separate the fibers, creating a local feature with a stress concentration,

$$k_t = \frac{\sigma_{max}}{\sigma_\infty} \tag{7}$$

where k_t is the stress concentration, σ_{max} is the maximum stress experienced at the local feature, and σ_∞ is the far field stress on the cloth. As an example $k_t = 3$ a discontinuity in the shape of a circle. In theory,

$$k_t = 1 + 2\frac{a}{b} \tag{8}$$

where $\frac{a}{b}$ is the ratio of the length of the width of a crack, and $a \gg b$. However, this is only an approximation. Using St. Venant's Principle, this increase in stress should have an impact only within a range of $5a$, or five times the length of the crack. Therefore, if the increased number of stitches per inch causes the effected areas to overlap, it should significantly effect the UTS.

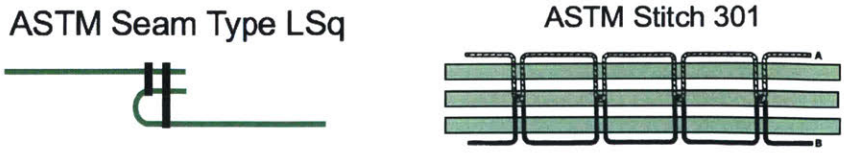
2.4 Thread Failure

Sections 2.2 and **2.3** discuss cloth failure. Alternatively, the thread could be the weakest link in the seam, and be the first to fail. In this case, the ultimate strength of the thread will be the determining factor. However, considering the thread in use is at thick as the fabric itself (which is the thickness of several fibers woven together), this is extremely unlikely, and preliminary studies have consistently shown that this is not the case.

3. Experimental Design

3.1 Sample Fabrication

Green EMMAKITES 40D Ripstop Nylon Fabric was cut into coupons on a paper cutter to ensure straight clean edges. The coupons were cut to arbitrary lengths, but the width was a constant, of 11 boxes of the grid on the material, approximately 1.62 in. All coupons were cut in the same orientation so that seams would fail in the warp direction of the fabric. Coupons were sewn together to create seams on on a SINGER Merrit 1872 sewing machine. The stitch concentration is defined as the number of stitches per inch**.** In order to adjust the stitch concentration, three different stitch size settings (1,2,and 3.5) were used on the sewing machine. Images of the different stitch concentration are shown in **Figure 3-2**. However, due to the the fact that these were manually assembled, the stitch concentration was variable even with the same stitch setting, particularly at smaller sizes. An ASTM 301 stitch was used on these seams to create a ASTM LSq seam, as shown in the figure below.



https://www.astm.org/Standards/D6193.htm

Figure 3-1: The ASTM stitch and seam used in testing. Stitch image modified from ASTM site.

The LSq seam was made by sewing one seam connecting the two pieces of fabric, then folding the fabric over and sewing the second stitch through three layers of fabric. The thread used was COATS & CLARK Dual Duty XP Heavy Thread.

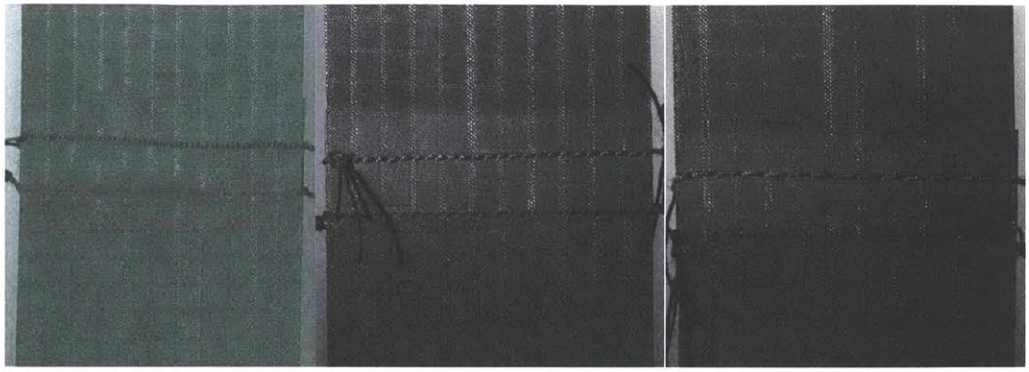


Figure 3-2: Three different stitch concentration, each sewn on a different setting on a SINGER Merrit 1872 sewing machine. The image on the left was sewn on setting one, the image in the center was sewn on 2, and the image on the right was sewn on setting 3.5.

3.2 Instron Testing

All testing was completed on an Instron 5582 (or "the Instron") using Bluehill software, in room number 1-307 at the Massachusetts Institute of Technology, in Cambridge, Massachusetts. The coupons were inserted into the jaws of the Instron and clamped down. Since this material has an especially low coefficient of friction, double-sided tape was placed on each sample before it was clamped into the Instron to provide added friction, and prevent slipping of the samples. Tests assessing the effects of stitch concentration were conducted at a constant displacement of 100mm/min. Strain rate tests were conducted at three different constant displacements: 100mm/min, 250mm/min, and 400mm/min. The length between the jaws was measured with calipers in order to determine a strain rate. The jaws move at a specified rate until either the force exceeds 2000N or the displacement exceeds 35mm. In each test, the line of stitches going through three pieces of cloth was closer to the moving jaw.

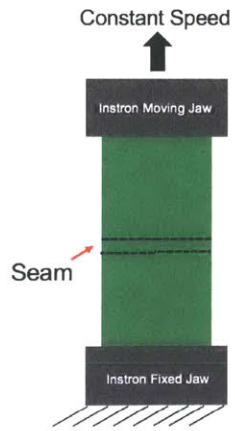


Figure 3-3: The cloth is secured in the two jaws of the Instron and the moving jaw ascends at a constant speed. The Instron records the force required to pull the cloth.

3.2 Vic2D and Ncorr Set-up

While the Instron was stretching the samples, a camera was set-up to take photographs every ½ of a second, using the program Vic-Snap 2010. These images were input to the open source Matlab function Ncorr, which, using digital image correlation provided a visualization of the strain. The "high strain" feature in Ncorr was used to accommodate the high strain of the cloth, and all recommended parameters were used.

4. Results

4.1 Instron Data

These experiments test the effect of stitch concentration and strain rate on seam efficiency. The results are shown in **Figures 4-1** through **4-13** below. **Figures 4-1** and **4-2** plot the seam efficiency, calculated from the UTS, against the strain rate and stitch concentration respectively. Over the range of strain rate tested, no curve was able to be fitted to the to the data.

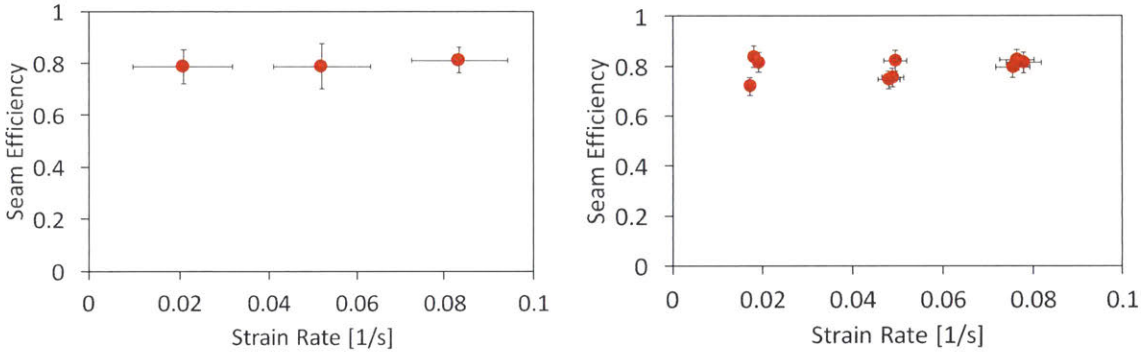


Figure 4-1: Seam efficiency as a function of strain rate. Data was collected by taking seam samples and stretching then at three different constant speeds (100mm/min, 250mm/min, 400mm/min). The graph on the left shows the average of each coupon tested at the same speed, and the graph on the right shows each test individually. No curve could be fitted to either of these graphs, indicating that over these ranges, the strain rate is not a relevant factor to properly calculating seam efficiency.

The effect of stitch concentration on seam efficiency, however was clear. While a T-Test of the samples between the two larger stitch concentration did not yield a statisticially different dataset, a T-Test between the smallest stitches and largest stitches yielded a statistically significant differece, with a $p=.0108$, indicating that the stitch concentration is a relevant factor to determining the seam efficiency. An equation fo the form

$$y = A - e^{-X/B} \tag{9}$$

was fit to the data collected. **Figure 4-2** shows both the fit and the data collected.

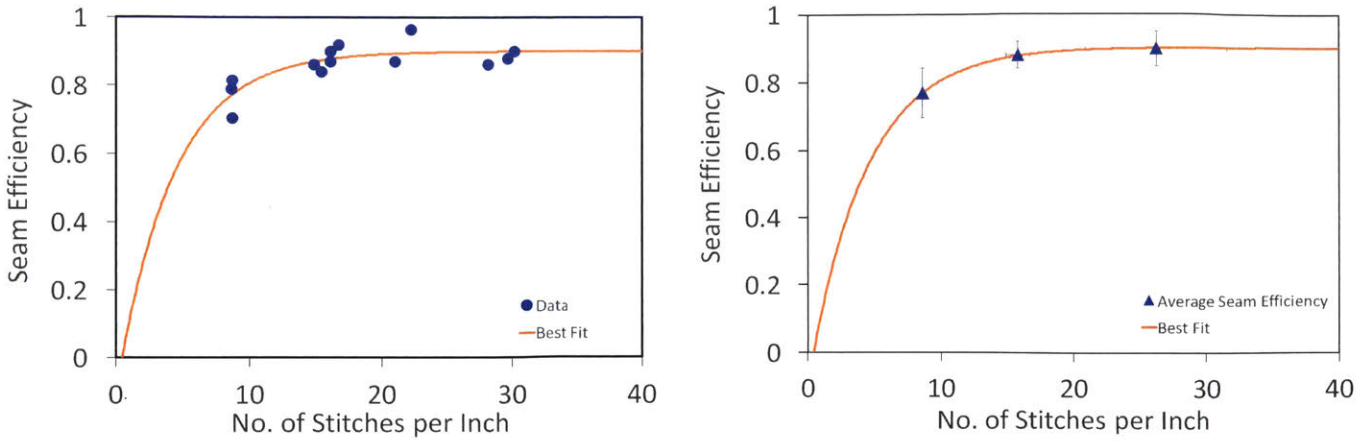


Figure 4-2: Seam efficiency as a function of stitch concentration. The graph on the right shows the average of each coupon sewn together on the same setting on the sewing machine, and the graph on the left shows each test individually. The orange line is the best fit of the data. On the left, the constant A=0.9008±0.04, on the right A=0.9003 ±0.01. The coefficient B for the graph on the left is 4.236±1.1 and the on the right is 4.235±0.4. The uncertainties were calculated with a 95% confidence. The R^2 value for the graph on the left is 0.80, and the graph on the right is 0.99.

This best fit line meets all of the expected results at edge cases. If A is less than or equal to one, then the seam efficiency can not exceed one, and it should drop to zero at zero stitches per inch.

The best fit curve for the raw data is

$$y = 0.9008 - e^{-x/4.236} \tag{10}$$

with an R^2 of .80. Uncertainties are in the **Figure 4-2** caption.

The best fit curve for the average of the raw data is

$$y = 0.9003 - e^{-x/4.235} \tag{11}$$

with an R^2 of .99. Uncertainties are in the **Figure 4-2** caption. **Figures 4-3** through **4-14** present the output of the digital image correlation.

4.2 Vic-Snap 2010 and Ncorr Visualizations

In **Figures 4-3** through **4-11,** the change in transverse, longitudinal, and shear Green-Lagrangian strain over the total test time are presented for one representative sample from each stitch size. Green Lagrangian strain, ε_G, is defined as:

$$\varepsilon_G = \frac{1}{2}(\lambda^2 - 1) \tag{12}$$

where λ is the ratio of final length to initial length. There are three general observations that can be seen from these images:

1.) As the stitch concentration increases, the strain in every direction shown decreases.

2.) In the longitudinal strain, it is clear that the center of the seam undergoes little to no strain.

3.) The strain in the transverse and shear direction are dynamic and changes both in position and magnitude, while the longitudinal strain changes mainly in magnitude.

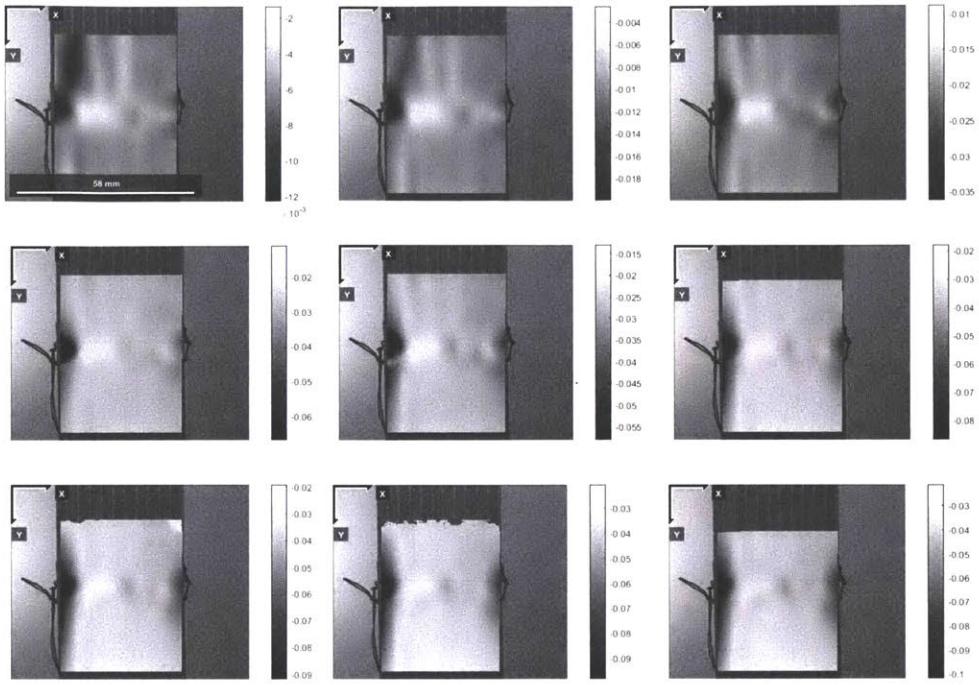


Figure 4-3: Visualization of strain in the ε_{xx} (transverse strain) of a sample with a stitch density of 29.6 ±0.2 stitches per inch and a cross head speed of 100mm/min through the test.

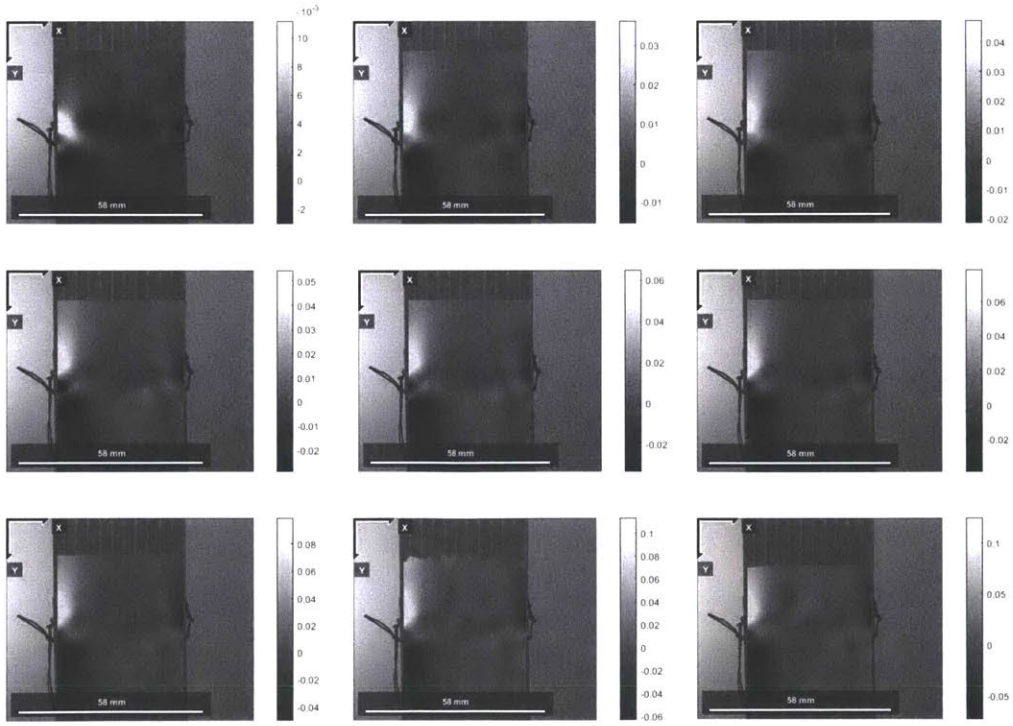


Figure 4-4: Visualization of strain in the ε_{xy} (shear strain) of a sample with a stitch density of 29.6 ±0.2 stitches per inch and a cross head speed of 100mm/min through the test.

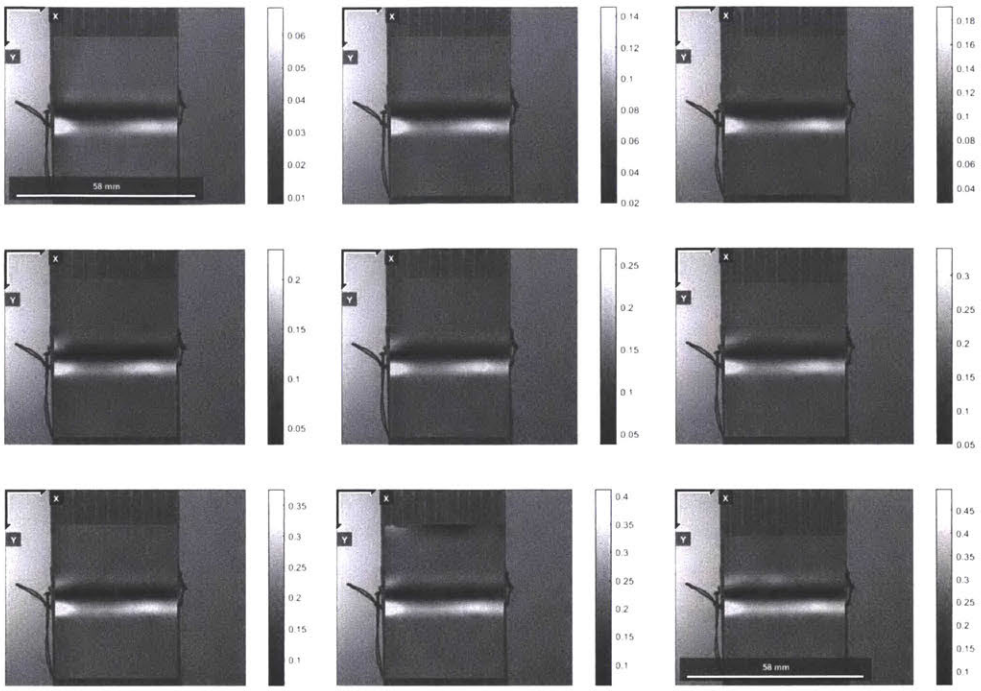


Figure 4-5: Visualization of strain in the ε_{yy} (longitudinal strain) of a sample with a stitch density of 29.6 ±0.2 stitches per inch and a cross head speed of 100mm/min through the test.

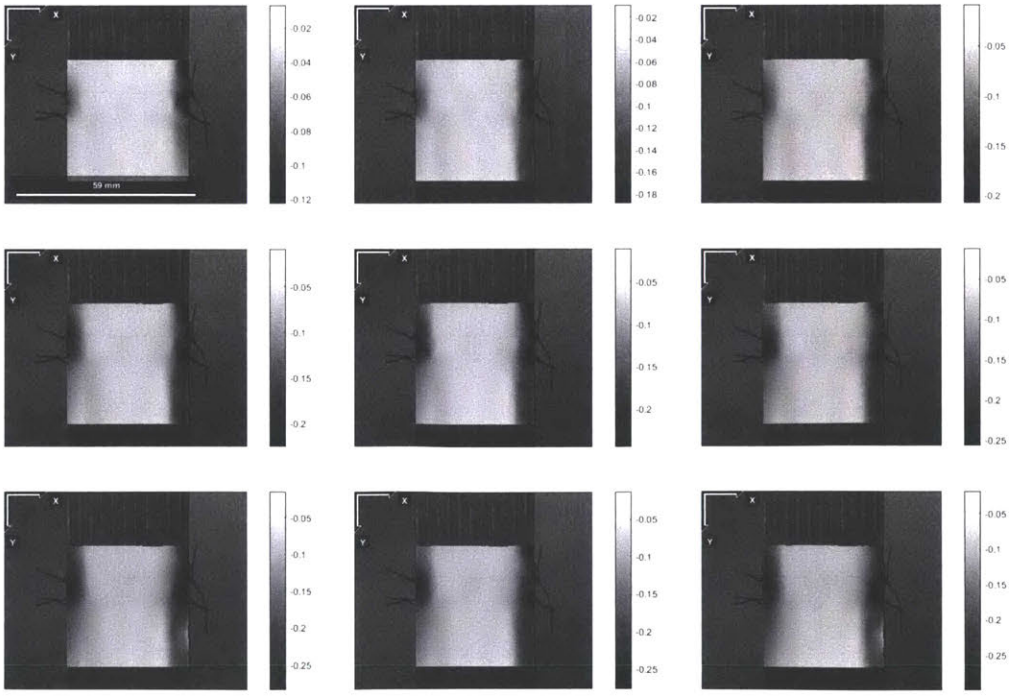


Figure 4-6: Visualization of strain in the ε_{xx} (transverse strain) of a sample with a stitch density of 15.4 ±0.1 stitches per inch and a cross head speed of 100mm/min through the test.

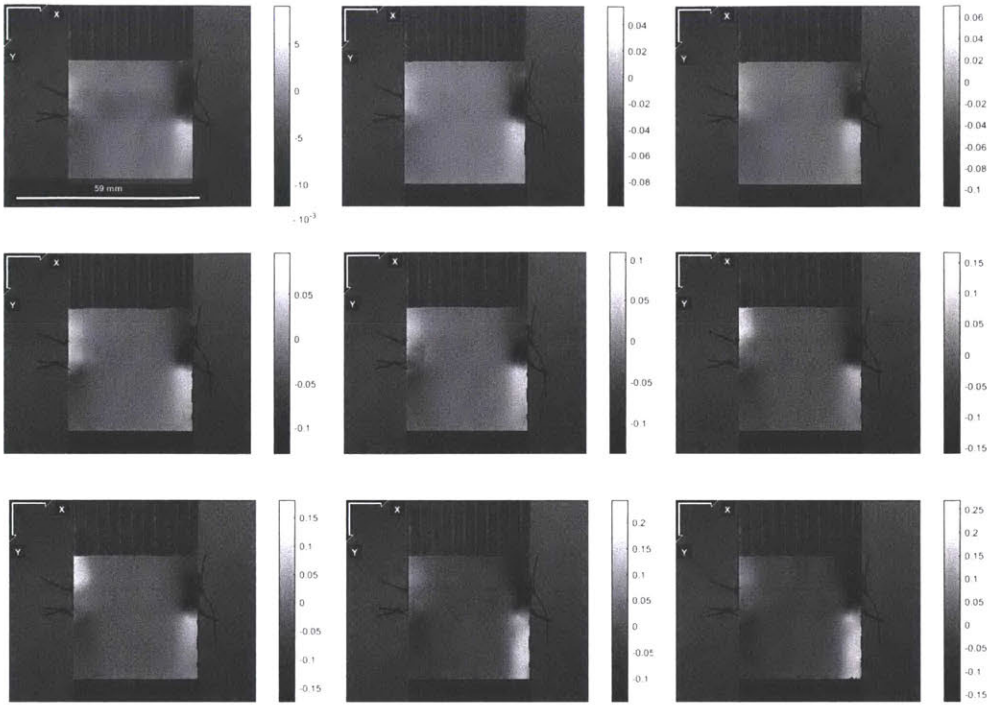


Figure 4-7: Visualization of strain in the ε_{xy} (shear strain) of a sample with a stitch density of 15.4 ±0.1 stitches per inch and a cross head speed of 100mm/min through the test.

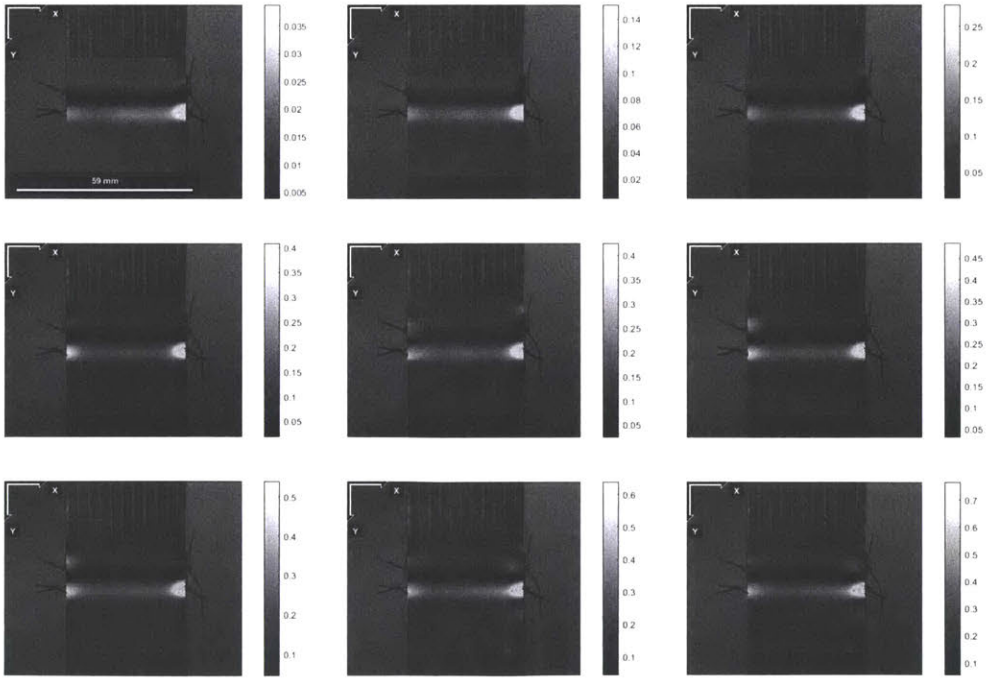


Figure 4-8: Visualization of strain in the ε_{yy} (longitudinal strain) of a sample with a stitch density of 15.4 ±0.1 stitches per inch and a cross head speed of 100mm/min through the test.

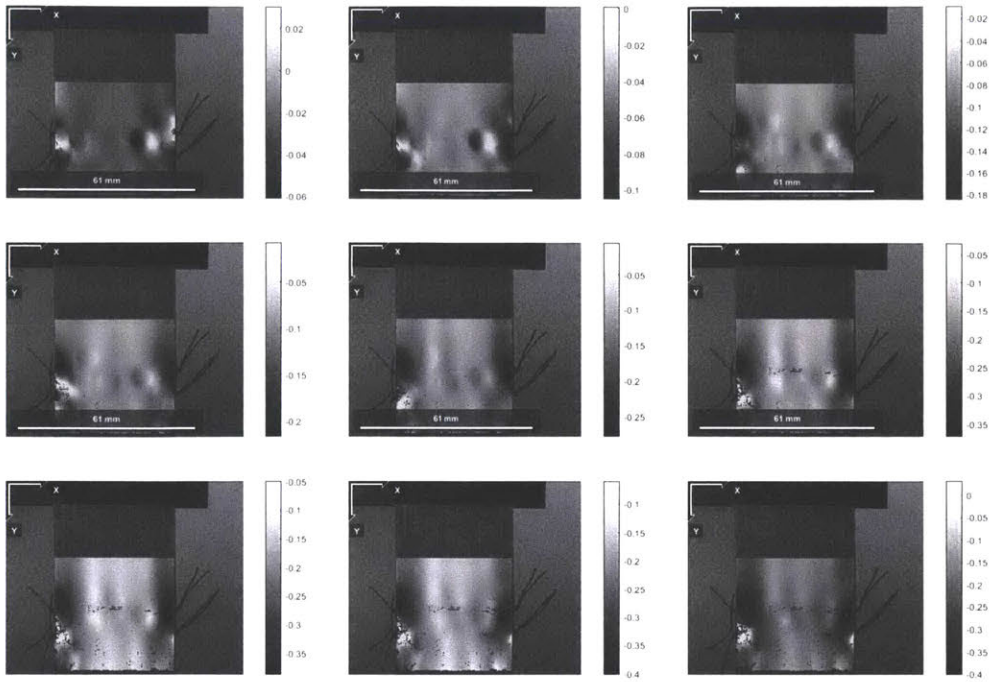


Figure 4-9: Visualization of strain in the ε_{xx} (transverse strain) of a sample with a stitch density of 8.67 ±0.02 stitches per inch and a cross head speed of 100mm/min through the test.

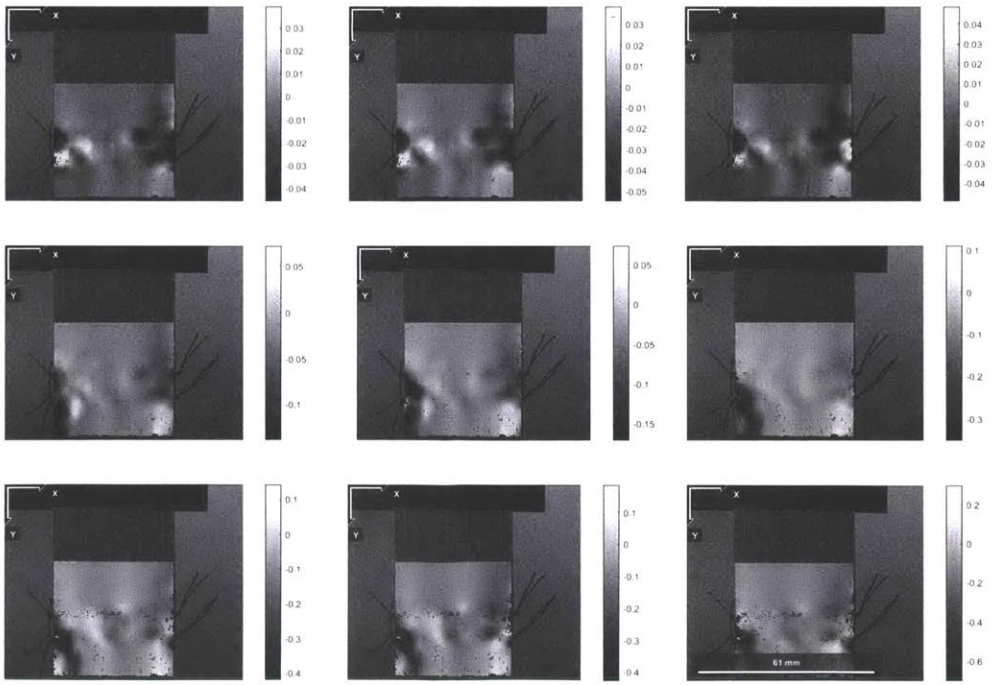


Figure 4-10: Visualization of strain in the ε_{xy} (shear strain) of a sample with a stitch density of 8.67 ±0.02 stitches per inch and a cross head speed of 100mm/min through the test.

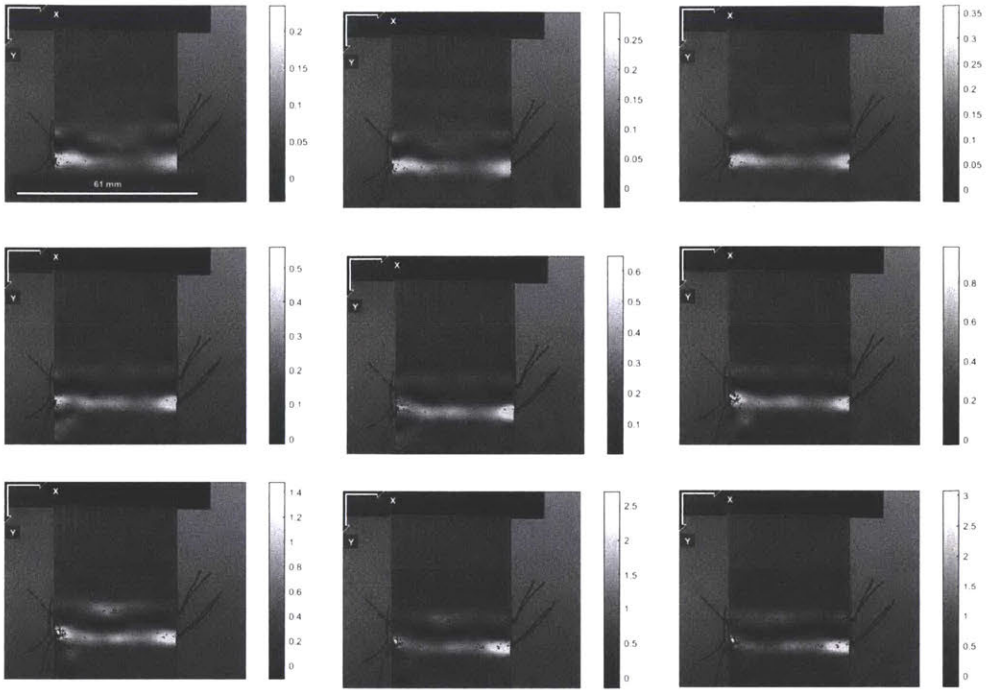


Figure 4-11: Visualization of strain in the ε_{yy} (longitudinal strain) of a sample with a stitch density of 8.67 ±0.02 stitches per inch and a cross head speed of 100mm/min through the test.

The the end of each test, the seam failed on its outer edges, highlighted in **Figures 4-5, 4-8,** and **4-11. Table 4-1** tabulates the failure mode of each of the samples tested.

Table 4-1: Stitches per inch, the calculated seam efficiency, and the failure mode of the seam are shown for the data presented in **Figure 4-2**. T, for top row of stitches, means that the seam failed at the row of stitches closer to the moving jaw. B, for bottom row of stitches means that the seam failed at the row of stitches closer to the fixed jaw.

Stitches per inch	Seam Efficiency	Failure Mode
29.6	0.86	T
22.2	0.94	B
21.0	0.85	B
30.1	0.88	T
28.1	0.84	T
16.7	0.90	B
14.8	0.84	T
16.0	0.85	B
16.0	0.88	B
15.4	0.82	B
8.64	0.80	B
8.67	0.69	B
8.59	0.77	T

The remaining **Figures 4-12** through **4-14** show the Green-Lagrangian strain in the last image recorded before failure for a representative sample in each stitch concentration. In addition, the maximum and minimum are marked with a green dot on each image. In combination with the data in **Table 4-1**, **Table 4-2** records whether the initial point of failure is identifiable from the locations maximum or minimum strain. Only in the longitudinal strain of the sample with 29.3 stitches per inch does the point of maximum strain not match the failure mode. **Figures 4-12** through **4-14**, it is also clear that with greater stitch concentration, there are greater strains in every direction. Additionally, the photograph also clearly shows that with lower stitch concentrations, an accordion-like crumpling occurs.

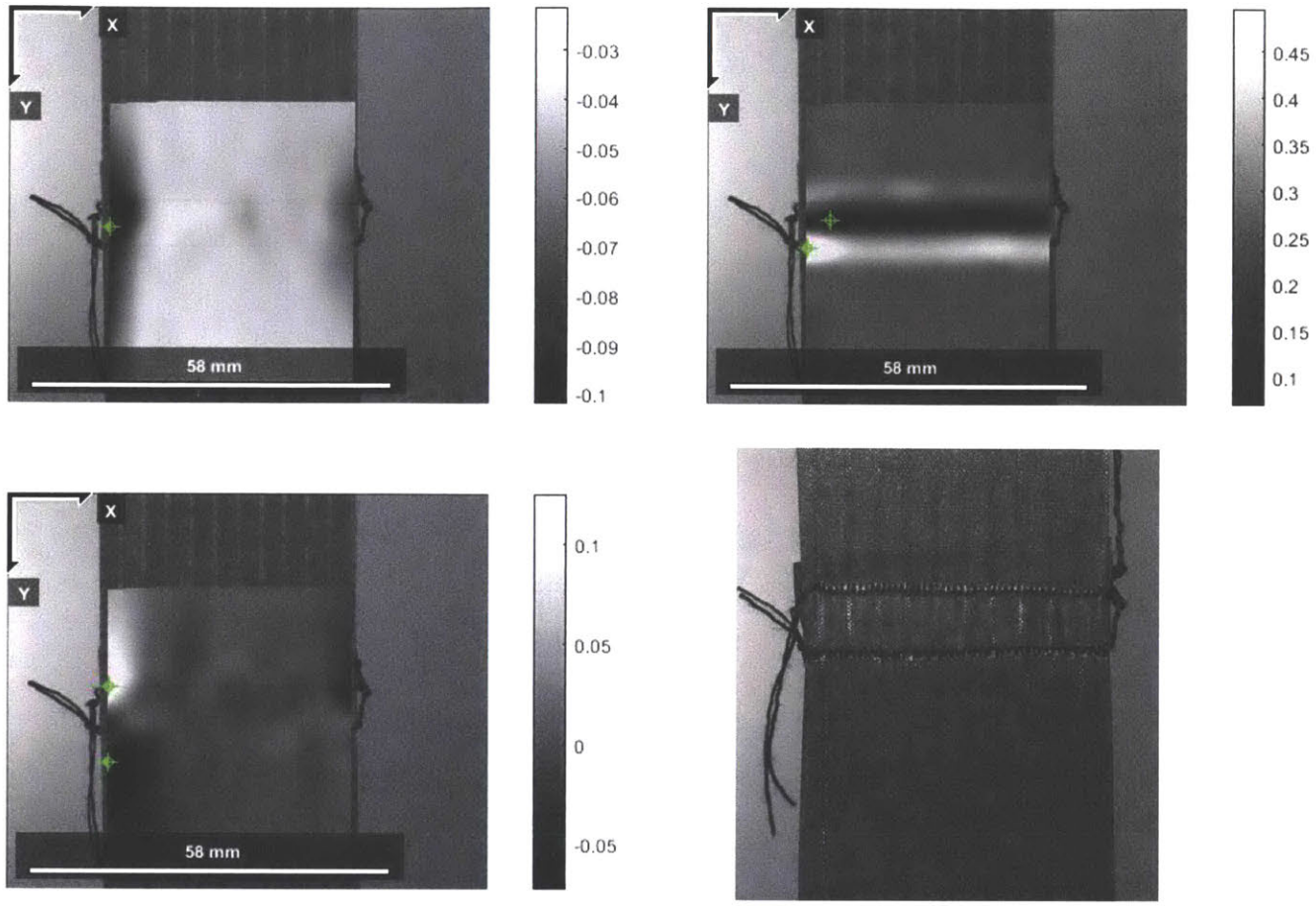


Figure 4-12: Visualization of strain in the ε_{xx} (top left), ε_{yy} (top right), and ε_{xy} (bottom left) just before failure of a sample with a stitch density of 29.6 ±0.2 stitches per inch and a cross head speed of 100mm/min. The bottom right shows the corresponding photograph immediately before failure. The maximum and minimum points are shown with green dots.

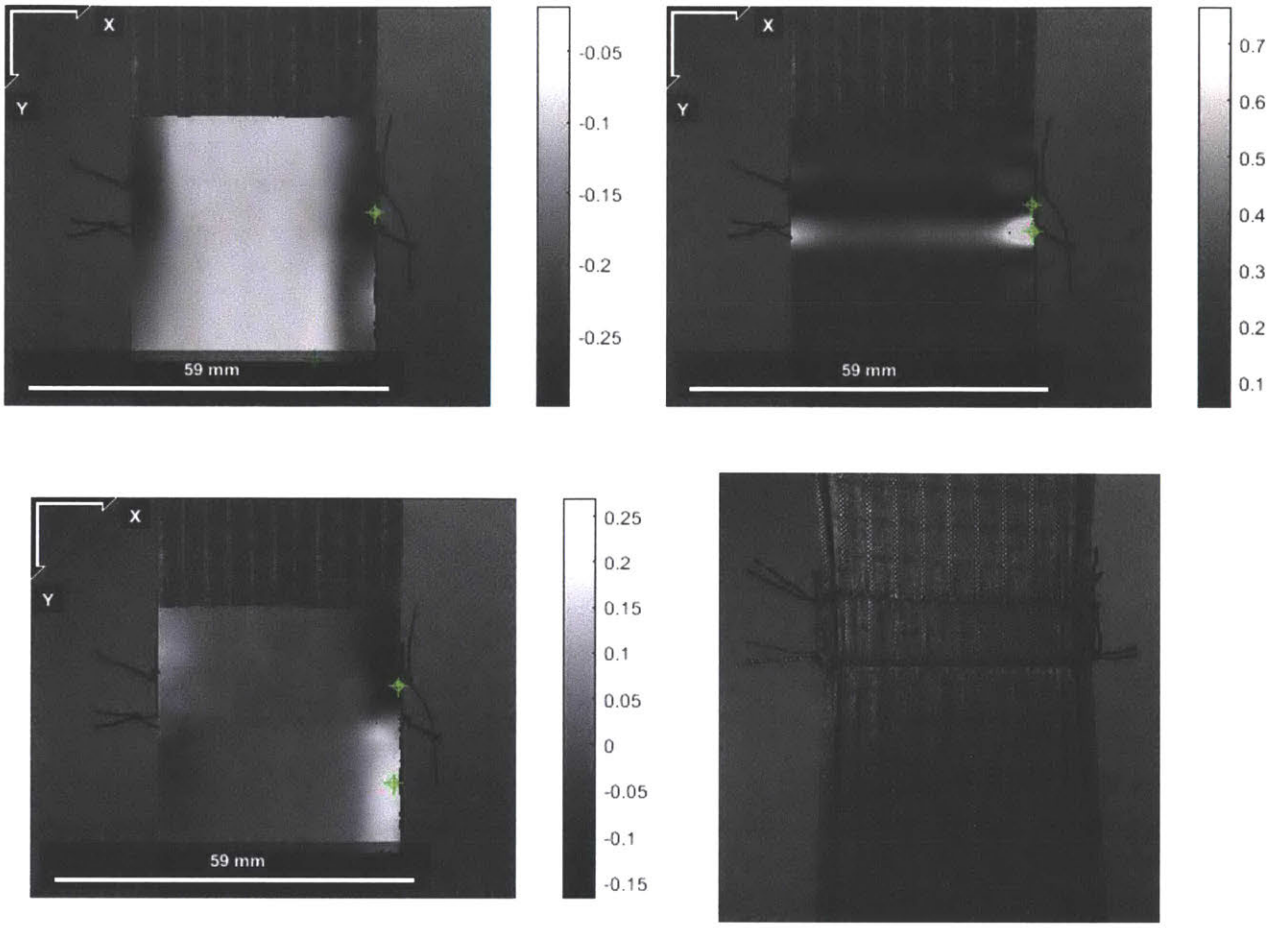


Figure 4-13: Visualization of strain in the ε_{xx} (top left), ε_{yy} (top right), and ε_{xy} (bottom left) just before failure of a sample with a stitch density of 15.4 ±0.1 stitches per inch and a cross head speed of 100mm/min. The bottom right shows the corresponding photograph immediately before failure. The maximum and minimum points are shown with green dots.

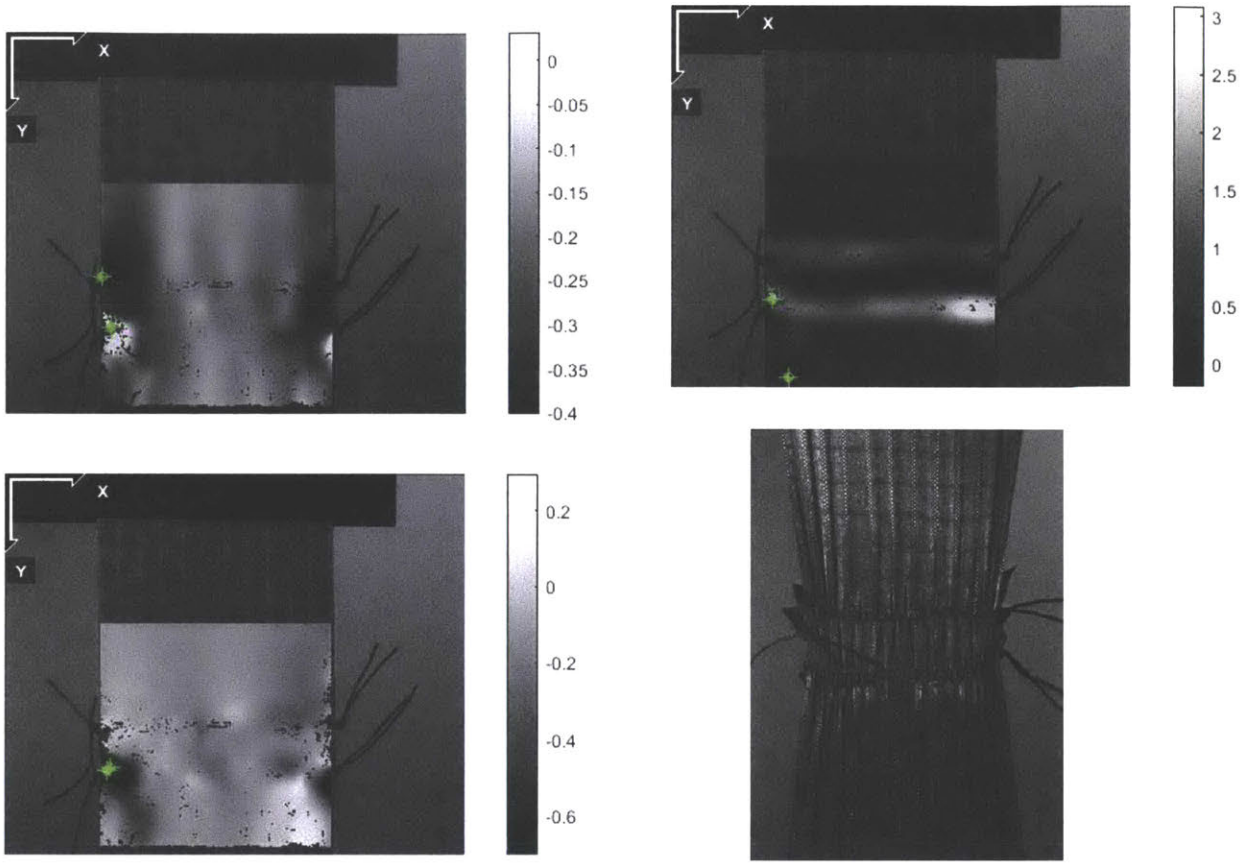


Figure 4-14: Visualization of strain in the ε_{xx} (top left), ε_{yy} (top right), and ε_{xy} (bottom left) just before failure of a sample with a stitch density of 8.67 ±0.02 stitches per inch and a cross head speed of 100mm/min. The bottom right shows the corresponding photograph immediately before failure. The maximum and minimum points are shown with green dots.

Table 4-2: This table shows whether the digital image correlation presents a maximum or minimum strain at the location of failure. T, for top row of stitches, means that the seam failed at the row of stitches closer to the moving jaw. B, for bottom row of stitches means that the seam failed at the row of stitches closer to the fixed jaw.

Stitches per inch	Failure Mode	Exx	Eyy	Exy
29.6	T	Y	N	Y
15.4	B	Y	Y	Y
8.67	B	Y	Y	Y

5. Discussion

5.1 Instron Data

The results of this work show that in the range of seam parameters tested, seam efficiency was independent of strain rate and depended strongly on the stitch concentration. Strain rate was tested on a range from 0 to less than 0.1 Hz, and seam efficiency was found to be independent in this study, but previous publications have found that seam efficiency is dependent on strain rate. However, these publications were testing with strains in the range of 12 Hz, almost two orders of magnitude larger than the values tested here.[12]

This study found that seam efficiency monotonically increases as a function of stitch concentrations. The form of the best fit line is shown in *Equation 9*, and the coefficients are shown with 95% confidence in the caption for **Figure 4-2.** This fit was found using stitch concentrations ranging from 8 stitches per inch to 30 stitches per inch, and therefore cannot be applied to other ranges without further testing. It is expected that as stitch concentration increases, the efficiency of the seam will at some point start to decrease, as described in sections 2.3. The maximum of approximately 30 stitches per inch was selected because that was the maximum stitch concentration the sewing machine used in this study could handle.

The maximum average seam efficiency was reported at the highest average stitch concentration of around 26 stitches per inch. This conflicts with literature which states that the optimal stitch concentration should be from 8-11 inches per inch. [8,9,12] This discrepancy may be accounted for by the difference in materials and by the paper's use of webbing within the seam. This leaves an avenue open for future work with similar tests, different types of materials, and the presence of webbing.

5.2 Ncorr and Images

The most apparent visual difference in photographs of each of the different stitch concentration, is the accordion-like crumpling that occurs, as shown in **Figure 5-1**

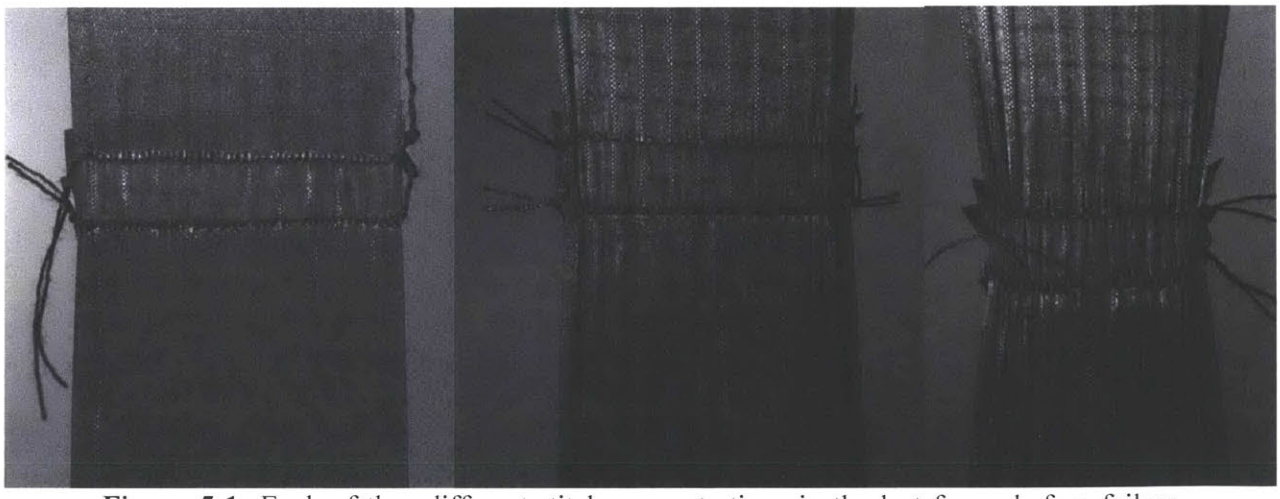


Figure 5-1: Each of thee different stitch concentrations in the last frame before failure showing the accordion-like crumpling.

This crumpling is characterized by ε_{xx} and ε_{xy}. In the Ncorr visualizations, the stress state in the transverse and shear strain underwent the most change throughout the test, while the longitudinal strain quickly developed a static stress state and then just grew in magnitude. One reason that may contribute to the difference between the change in strain state over the testing period in transverse and shear stress is the fact that these samples were assembled by hand, causing slight variability. Another reason is that because these strains are both dependent on the weft direction of the cloth, its fibers are more curved and also slightly weaker than in the warp, making it more likely for strain to occur. The most convincing reason, however, has to do with the load path of a seam.

In a seam, a single stitch will poke a hole through the cloth, separating fibers that use to be tightly intertwined. The thread will then pull downwards onto the weft threads that are normal to the direction of the stitch. In each Ncorr images, the location of failure is also characterized by a negative transverse and shear strain. As the stitches squish together, what use to be taught weft lines are now looser sagging weft lines that the downward force of the tread can easily apply force to and accentuate strain the the longitudinal direction, ultimately causing strain and failure at that location. Perhaps this is why these two transverse and shear strain across all three samples accurately located the point of failure, while the longitudinal stress did not.

6. Conclusions

The purpose of the study was to determine the affect of stitch concentration and strain rate on seam efficiency. This was assessed using an Instron 5582 to tear sample coupons to failure, and using the open source software Ncorr, to visualize the strain on the tested coupons. The conclusions of this study are succinctly summarized below.

1.) Seam efficiency is independent of strain rate for the ranges tested.

2.) Seam efficiency is dependent on concentration ranges tested.

3.)Seam efficiency has R^2=.99 for the the equation: $y = 0.9003 - e^{-x/4.235}$

4.) Transverse strain and shear strain are the most accurate ways to predict the failure location.

5.) The accordion-like crumpling has a significant impact on failure stress by causing larger

displacements in the longitudinal direction.

6.) The seams have an area of little to no strain at the center.

Works Cited

[1] L. White, "The Invention of the Parachute" Technology and Culture 9(3) (1968): 462-467.

[2] S. Lingard, "7 - Parachutes for space use," *Nasa Parachute. Seminar.*, 2005.

[3] H. Aeronautics, "Drag Characteristics of a Disk-Gap-Band Parachute With a Nominal Diameter of 1.65 Meters," *Security*, no. October, 1972.

[4] "NASA - Mars Parachute Testing in World's Largest Wind Tunnel", Nasa.gov, 2017. [Online]. Available: https://www.nasa.gov/mission_pages/mars/images/msl0164-20090422.html. [Accessed: 18- May- 2017].

[6] C. L. Tanner, C. O. Farrell, J. C. Gallon, and I. G. Clark, "Pilot Deployment of the LDSD Parachute via a Supersonic Ballute," pp. 1–22.

[5] V. L. Behr and S. Lingard, "Parachute Definitions, Parachute Definitions, Nomenclature, and Types Nomenclature, and Types." https://solarsystem.nasa.gov/docs/02%20Definitions%20Nomenclature%20and%20Types %20Lingard.pdf. [Accessed: 18- May- 2017].

[6] K. Weiss, "Parachute Design." 2017. [Online]. Available: http://www.hsl.org.au/articles/parachutes.pdf. [Accessed: 18- May- 2017].

[7] "A study of parachute seam design criteria. Part I, Investigation of the strength of nylon and rayon cloth seams :: Parachute History Collection", Lhldigital.lindahall.org, 2017. [Online]. Available: http://lhldigital.lindahall.org/cdm/ref/collection/parachute/id/914. [Accessed: 18- May- 2017].

[8] A. R. T. If and C. R. Miller, "A study of parachute seam design criteria. Part II - Investigation of the Strength of Nylon Webbing Joints," no. June, 1956.

[9] D. V. Kirubakar, I. Journal, E. Technology, D. V. K. Raj, and M. R. Devi, "Performance Analysis Of The Mechanical Behaviour Of Seams With Various Sewing Parameters For Nylon Canopy Fabrics," Vol. VII, no. Ii, 2016.

[10] V. L. Alley and R. W. Faison, "Experimental investigation of strains in fabric under biaxial and shear forces," *J. Aircr.*, vol. 9, no. 1, pp. 55–60, 1972.

[11] K. W. Gwinn, J. J. Totten, and D. E. Waye, "High Strain-Rate Testing Of Parachute Materials* Kenneth W. Gwinn John J. Totten Donald E. Waye."

[12] D. H. Brain, "35—the Prediction of Strengths of Lockstitch Seams in Woven Fabrics," *J. Text. Inst.*, vol. 61, no. 10, pp. 493–505, 1970.